비접촉 동력전달용 자기장치의 성능예측을 위한 해석법

최 장영

충남대학교 전기공학과

Contents

I Introduction

I. Introduction

Fig. Mechanical Couplings

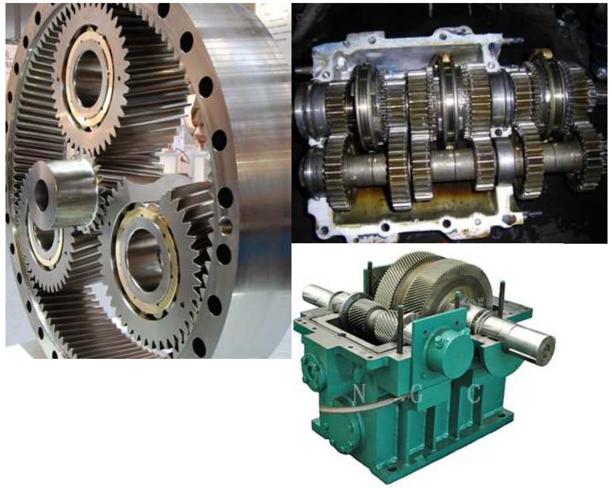

Fig. Mechanical Gears

- Couplings are mechanical devices for torque transmission in various industrial applications.
- Conventional couplings called mechanical coupling impart torque though mechanical contacts between separated parts.
- Maintenance is essential to prevent wearing down and destruction. Usually, mechanical couplings can be damaged in case of torque overload.

http://www.alfabb.com/
http://www.ptreview.co.uk/

I. Introduction

Fig. Broken mechanical couplings

Fig. Broken mechanical gears

http://machinedesign.com/

I. Introduction

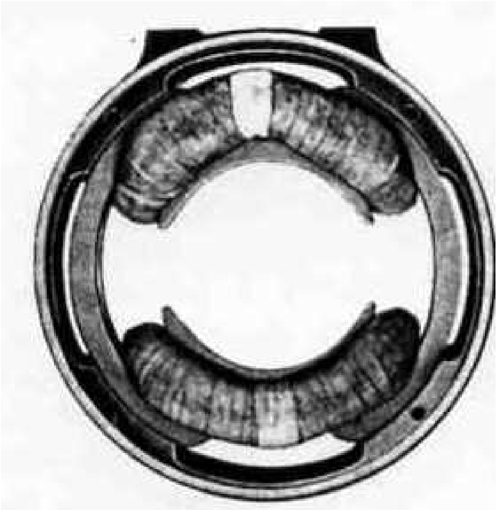

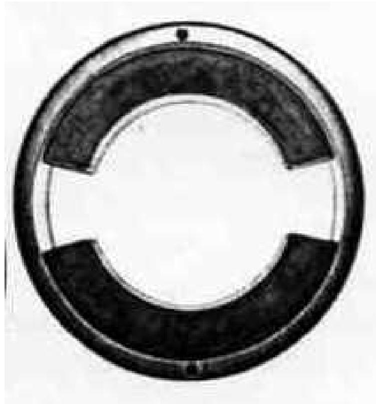

Reference : Irving M. Gottlieb (1982) - “Electric Motors & Control Techniques”

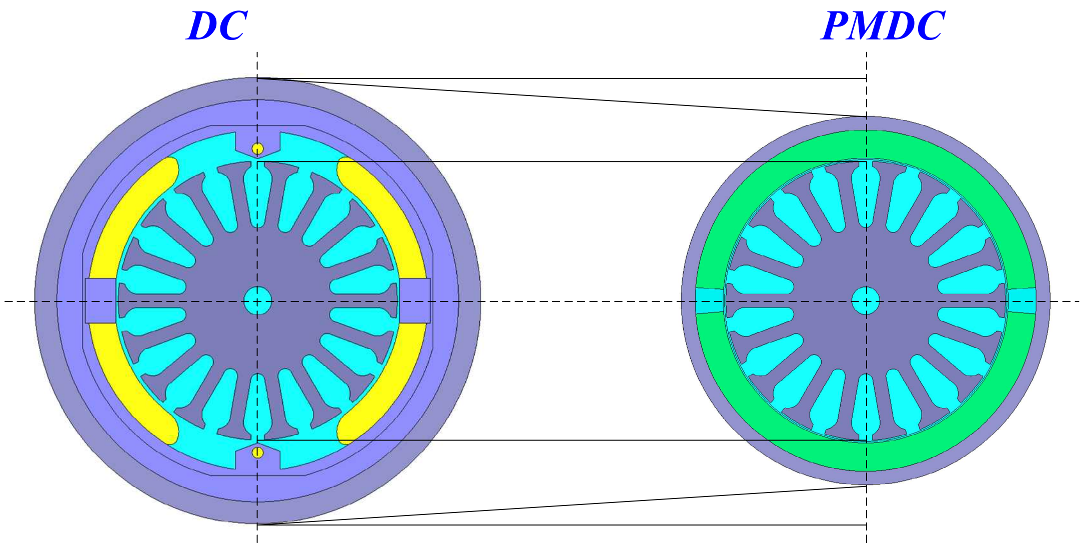

Reference : Robert C. Perrine (1999) - “Design Handbook for PM Motors and Tachometers”

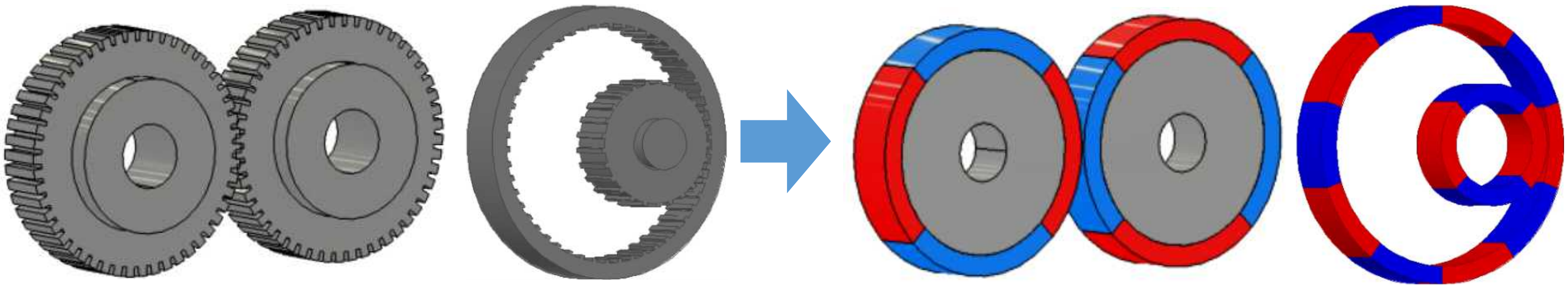

(a) (b)

Fig. Structure of (a) Mechanical gears (b) Magnetic gears

- Advantages of magnetic gear

✓ Physical isolation
✓ Low maintenance
✓ Silent operation
✓ Inherent overload protection

I. Introduction

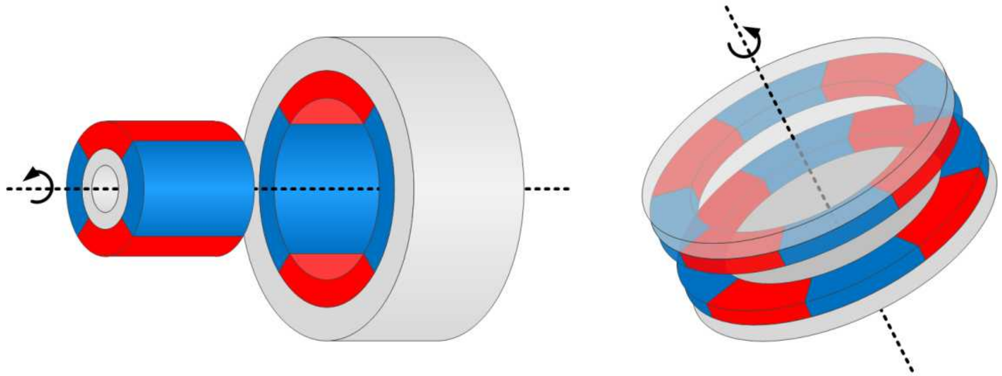

(a) (b)

Fig. Structures of couplings: (a) RFPM (b) AFPM

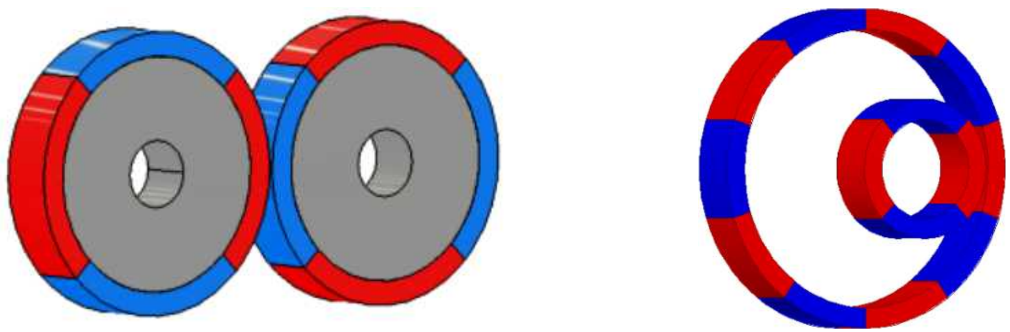

(a) (b)

Fig. Structures of gears: (a) Spur (b) Cycloid

Governing Equations

$$\mathbf{B} = \mu_0 (\mathbf{H} + \mathbf{M})$$

$$\nabla \times \mathbf{B} = \mu_0 \nabla \times \mathbf{H} + \nabla \times \mu_0 \mathbf{M}, \xrightarrow{\nabla \times \mathbf{H} = \mathbf{J} = 0} \nabla \times \mathbf{B} = \nabla \times \mu_0 \mathbf{M},$$

$$\mathbf{B} \equiv \nabla \times \mathbf{A}$$

$$\nabla \cdot \mathbf{A} = 0$$

$$\nabla^2 \mathbf{A} = -\mu_0 (\nabla \times \mathbf{M})$$

II Analytical Approach - Couplings

II. Analytical Approach – RFPM Coupling

A. Analytical Model

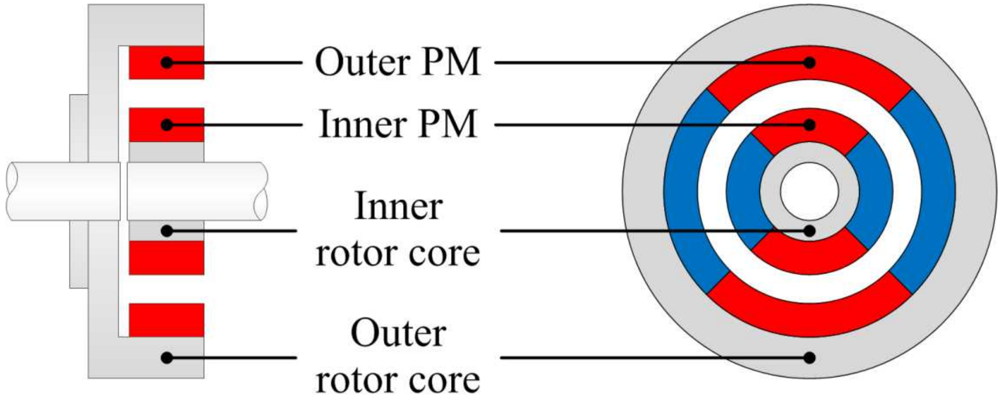

Fig. Schematic diagram of RFPM Coupling

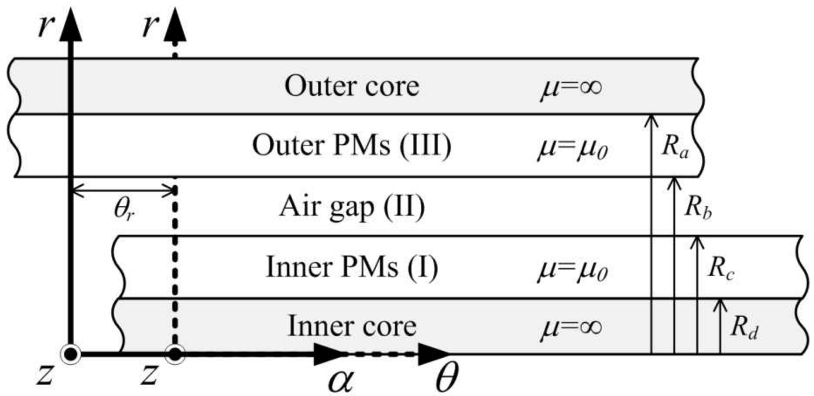

Fig. Analytical Model

II. Analytical Approach – RFPM Coupling

B. Magnetization

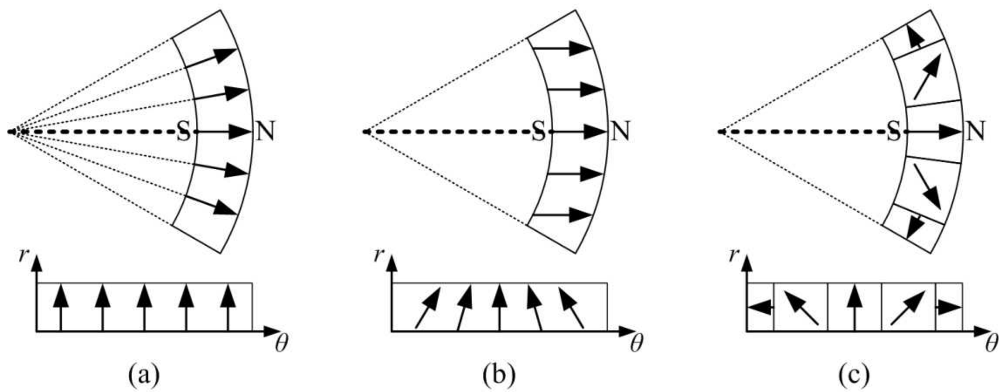

Fig. Possible Magnetization Patterns: (a) radial, (b) parallel, (c) Halbach

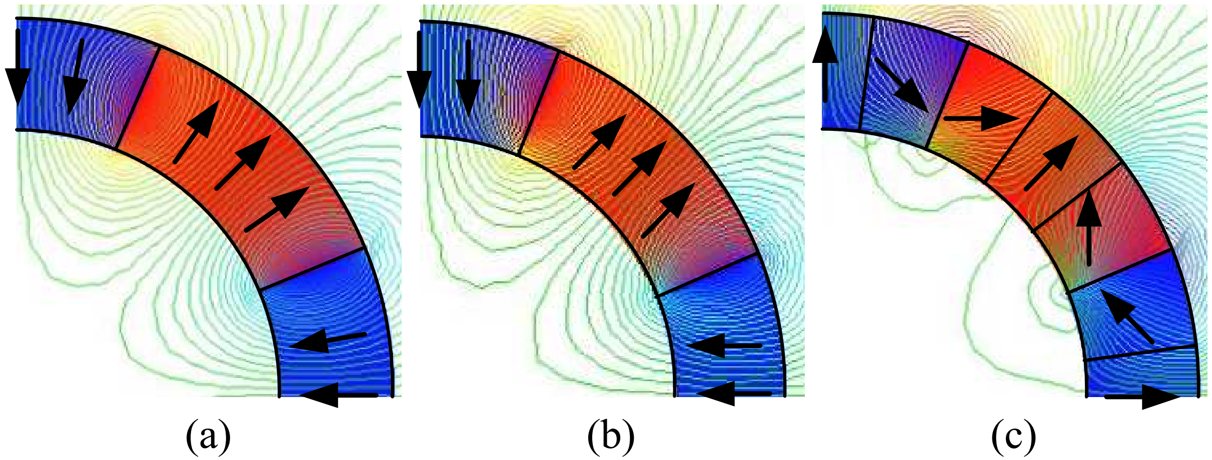

Fig. Magnetization Patterns : (a) radial magnetization (b) parallel magnetization (c) 3-segments Halbach magnetization

B. Magnetization

1) Radial magnetization

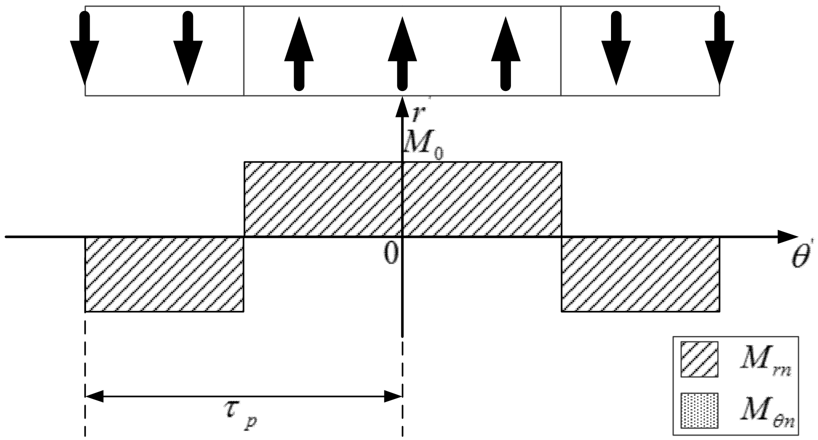

Fig. Radial magnetization model for Fourier series expansion

$$\vec{M} = \sum_{n=-\infty, odd}^{\infty} M_{rn} e^{-jnp_s\theta'} \mathbf{i_r}$$

$$M_{rn} = \frac{jM_o}{n\pi} \left(e^{-jn\pi\theta_p/2p_s} - e^{jn\pi\theta_p/2p_s}\right)$$

B. Magnetization

2) Parallel magnetization

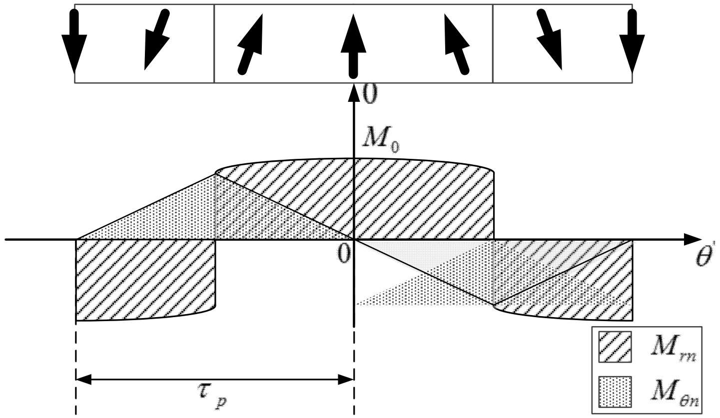

Fig. Parallel magnetization model for Fourier series expansion

$$\vec{M} = \sum_{n=-\infty, odd}^{\infty} (M_{rn}\mathbf{i_r} + M_{\theta n}\mathbf{i_\theta}) e^{-jnp_s\theta'}$$

$$M_{\theta n} = \frac{M_0 p_s}{\pi\{1-(np)^2\}} \left\{ \begin{aligned} & e^{jnp_s\theta_p/2}\left(\cos\frac{\theta_p}{2} - jnp\sin\frac{\theta_p}{2}\right) \\ & -e^{-jnp_s\theta_p/2}\left(\cos\frac{\theta_p}{2} + jnp\sin\frac{\theta_p}{2}\right) \end{aligned} \right\}$$

$$M_{rn} = \frac{M_0 p_s}{\pi\{1-(np)^2\}} \left\{ \begin{aligned} & e^{jnp_s\theta_p/2}\left(\sin\frac{\theta_p}{2} + jnp\cos\frac{\theta_p}{2}\right) \\ & -e^{-jnp_s\theta_p/2}\left(-\sin\frac{\theta_p}{2} + jnp\cos\frac{\theta_p}{2}\right) \end{aligned} \right\}$$

II. Analytical Approach – RFPM Coupling

B. Magnetization

3) Halbach magnetization

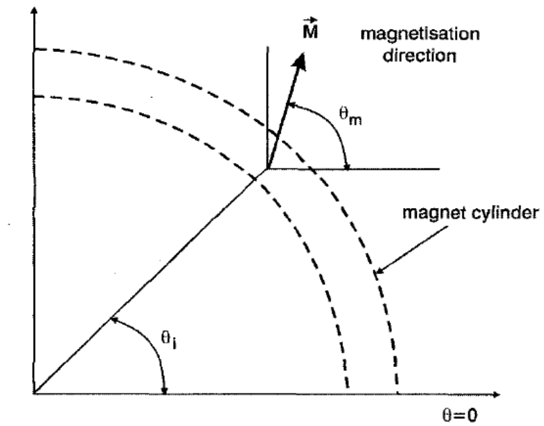

Fig.2 *Angular relationship between θ_m and θ_i*

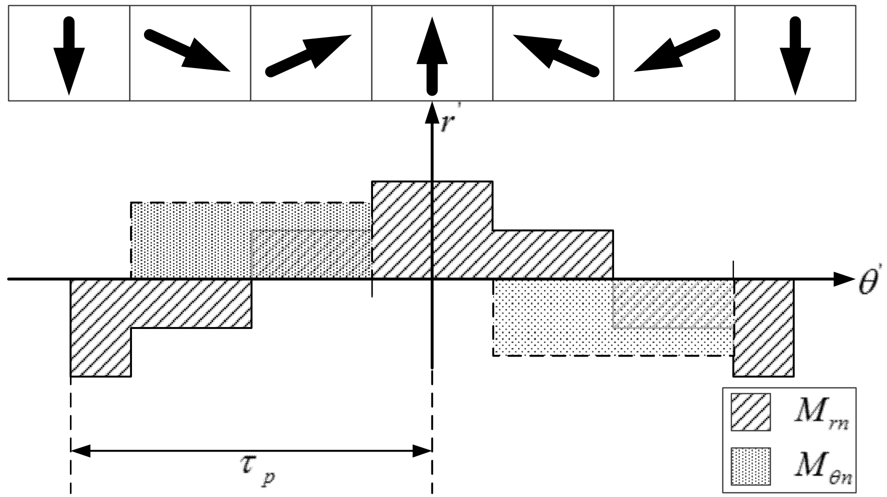

Fig. 3-segments Halbach magnetization model for a Fourier series expansion

$$\theta_m = (1 \pm p)\theta_i,$$

where θ_m and θ_i represent the direction of each individual magnet segment and the angle between criterion of angle (θ=0) and the center of the ith magnet segment, respectively.

$$\mathbf{M} = \sum_{n=-\infty,odd}^{\infty} (M_{rn} \cdot \mathbf{i_r} + M_{\theta n} \cdot \mathbf{i}_\theta) \cdot e^{-jnp_s\theta}$$

$$M_{rn} = \frac{M_0}{2\beta_p}\left\{ e^{\frac{5\beta_p}{6}} - e^{-\frac{5\beta_p}{6}} + e^{\frac{\beta_p}{6}} - e^{-\frac{\beta_p}{6}} \right\} + \frac{M_0}{\beta_p}\left\{ e^{-\beta_p} - e^{\beta_p} + e^{7\beta_p} + e^{5\beta_p} \right\}$$

$$M_{\theta n} = \frac{\sqrt{3}M_0}{4\beta_p}\left\{ e^{\frac{5\beta_p}{6}} + e^{-\frac{5\beta_p}{6}} - e^{\frac{\beta_p}{6}} - e^{-\frac{\beta_p}{6}} \right\}$$

Z. Q. Zhu and D. Howe, "Halbach permanent magnet machines and applications: a review," *IEE Proc.-Electr. Power Appl.*, vol. 148, pp. 299-308, Jul. 2001.

II. Analytical Approach – RFPM Coupling

B. Governing Equations

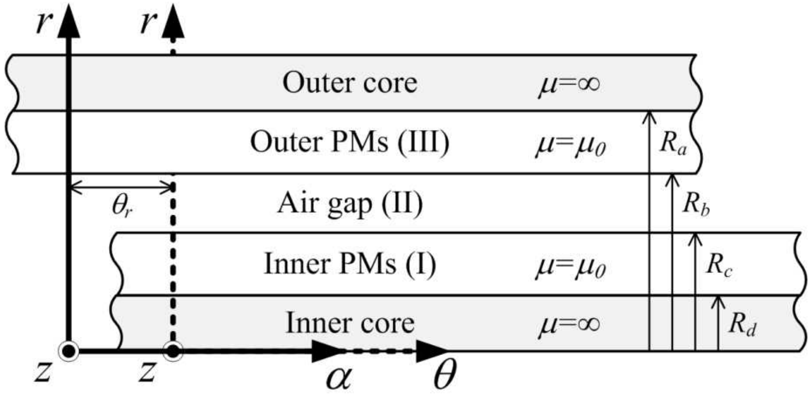

$$\nabla^2 \mathbf{A}^{\mathbf{I,III}} = -\mu_0 \left(\nabla \times \mathbf{M}_{\mathbf{RF}}^{\mathbf{in,out}} \right)$$

$$\nabla^2 \mathbf{A}^{\mathbf{II}} = 0$$

$$\mathbf{A} = \sum_{n=-\infty,odd}^{\infty} A_n(r) e^{-jnp(\alpha \,\mathrm{or}\, \theta)} \mathbf{i_z}$$

$$\nabla \times \mathbf{M}_{\mathbf{RF}}^{\mathbf{in,out}} = \frac{1}{r} \begin{vmatrix} \mathbf{i_r} & r\mathbf{i_\theta} & \mathbf{i_z} \\ \dfrac{\partial}{\partial r} & \dfrac{\partial}{\partial \theta} & \dfrac{\partial}{\partial z} \\ \displaystyle\sum_{n=-\infty,odd}^{\infty} M_{rn}^{in,out} e^{-jnp(\alpha \,\mathrm{or}\, \theta)} & \displaystyle\sum_{n=-\infty,odd}^{\infty} rM_{\theta n}^{in,out} e^{-jnp(\alpha \,\mathrm{or}\, \theta)} & 0 \end{vmatrix}$$

$$= \sum_{n=-\infty,odd}^{\infty} \frac{np}{r} \left(\frac{M_{\theta n}^{in,out}}{np} + jM_{rn}^{in,out} \right) e^{-jnp(\alpha \,\mathrm{or}\, \theta)} \mathbf{i_z}$$

$$\frac{\partial^2}{\partial r^2} A_n^{I,III}(r) + \frac{1}{r}\frac{\partial}{\partial r} A_n^{I,III}(r) - \frac{(np)^2}{r^2} A_n^{I,III}(r) = -\frac{\mu_0 np}{r} M_n^{in,out}$$

$$\frac{\partial^2}{\partial r^2} A_n^{II}(r) + \frac{1}{r}\frac{\partial}{\partial r} A_n^{II}(r) - \frac{(np)^2}{r^2} A_n^{II}(r) = 0$$

$$\mathbf{A^I} = \sum_{n=-\infty,odd}^{\infty} \left\{ C_n^I r^{np} + D_n^I r^{-np} + \mu_0 r \frac{np}{(np)^2 - 1} M_n^{in} \right\} e^{-jnp\theta} \mathbf{i_z}$$

$$\mathbf{A^{II}} = \sum_{n=-\infty,odd}^{\infty} \left\{ C_n^{II} r^{np} + D_n^{II} r^{-np} \right\} e^{-jnp\alpha} \mathbf{i_z}$$

$$\mathbf{A^{III}} = \sum_{n=-\infty,odd}^{\infty} \left\{ C_n^{III} r^{np} + D_n^{III} r^{-np} + \mu_0 r \frac{np}{(np)^2 - 1} M_n^{out} \right\} e^{-jnp\alpha} \mathbf{i_z}$$

$$\mathbf{B} = \nabla \times \mathbf{A} = \frac{1}{r} \begin{vmatrix} \mathbf{i_r} & r\mathbf{i_\theta} & \mathbf{i_z} \\ \dfrac{\partial}{\partial r} & \dfrac{\partial}{\partial \theta} & \dfrac{\partial}{\partial z} \\ 0 & 0 & \displaystyle\sum_{n=-\infty,odd}^{\infty} A_n(r) e^{-jnp(\alpha \,\mathrm{or}\, \theta)} \end{vmatrix}$$

$$\mathbf{B_\theta} = -\sum_{n=-\infty,odd}^{\infty} \frac{\partial}{\partial r} A_n(r) e^{-jnp(\alpha \,\mathrm{or}\, \theta)} \mathbf{i_\theta}$$

$$\mathbf{B_r} = -\sum_{n=-\infty,odd}^{\infty} \frac{jnp}{r} A_n(r) e^{-jnp(\alpha \,\mathrm{or}\, \theta)} \mathbf{i_r}$$

II. Analytical Approach – RFPM Coupling

C. Boundary Conditions

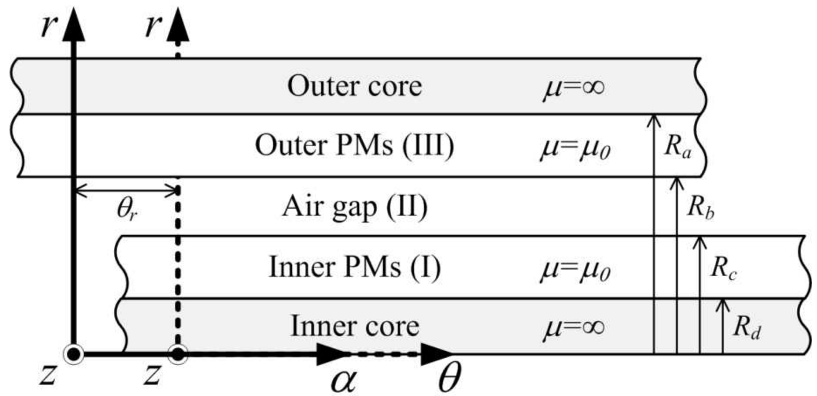

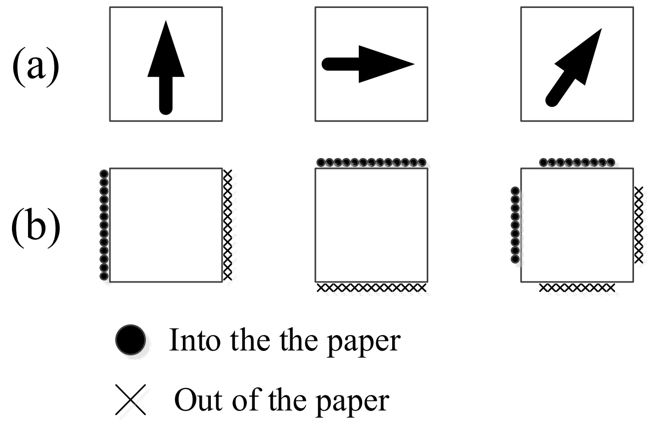

$$H_{\theta n}^{III}(R_b,\alpha) - H_{\theta n}^{II}(R_b,\alpha) = M_{\theta nn}^{out}$$

$$H_{\theta n}^{I}(R_c,\theta) - H_{\theta n}^{II}(R_c,\alpha) = M_{\theta nn}^{in}$$

$$\mathbf{B}_{\mathbf{r}}^{\mathbf{II}}(R_b,\alpha) = \mathbf{B}_{\mathbf{r}}^{\mathbf{III}}(R_b,\alpha)$$

$$\mathbf{B}_{\mathbf{r}}^{\mathbf{I}}(R_c,\theta) = \mathbf{B}_{\mathbf{r}}^{\mathbf{II}}(R_c,\alpha)$$

$$\mathbf{B}_{\boldsymbol{\theta}}^{\mathbf{I}}(R_d,\theta) = 0$$

$$\mathbf{B}_{\boldsymbol{\theta}}^{\mathbf{III}}(R_a,\alpha) = 0$$

$$\mathbf{F} = -S_{RF}\mu_0 \left\langle \mathbf{H}_{\mathbf{r}}^{\mathbf{II}}(R_b,\alpha,z)\mathbf{H}_{\boldsymbol{\theta}}^{\mathbf{II}}(R_b,\alpha,z) \right\rangle_{\alpha}$$

$$= -\frac{S_{RF}}{\mu_0}\left[\mathbf{B}_{\mathbf{r}}^{\mathbf{II}}(R_b,\alpha,z)\cdot\left\{ \mathbf{B}_{\boldsymbol{\theta}}^{\mathbf{II}}(R_b,\alpha,z) \right\}^{*} \right]$$

D. Results

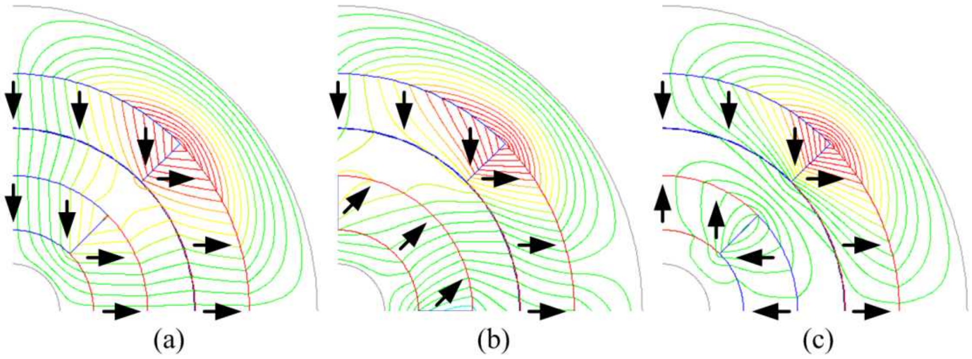

Fig. Magnetic flux line distribution of parallel RFPMC according to relative angular shift: (a) θ_r = 0°, (b) θ_r = 45°, and (c) θ_r = 90°.

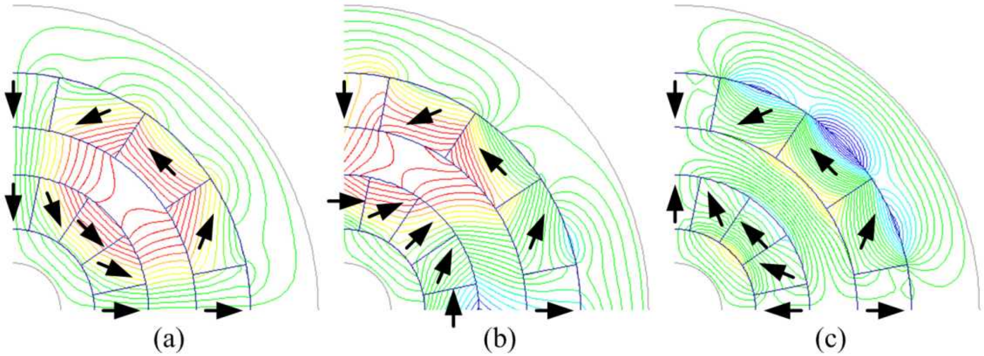

Fig. Magnetic flux line distribution of Halbach RFPMC acording to relative angular shift: (a) θ_r = 0°, (b) θ_r = 45°, and (c) θ_r = 90°.

II. Analytical Approach – RFPM Coupling

D. Results

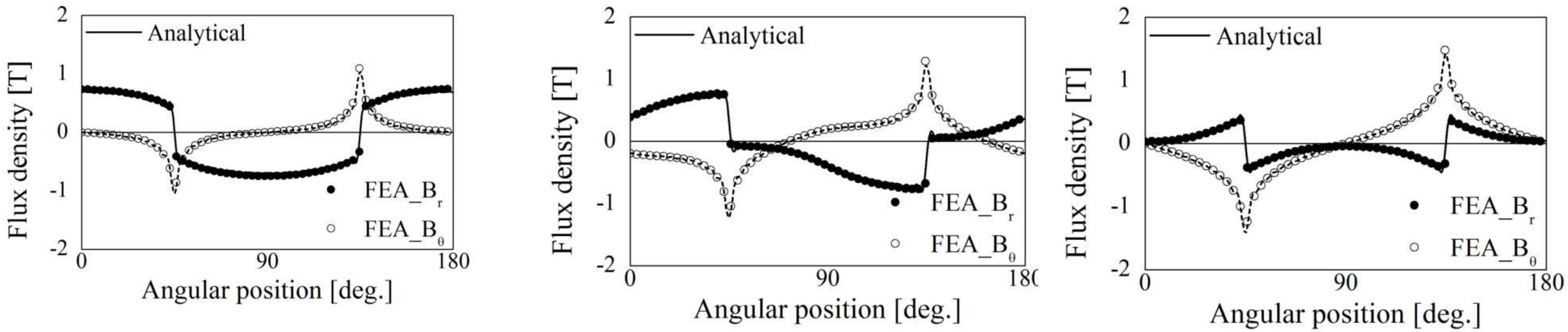

Fig. Comparison of analytical results with FE results for air gap flux density of parallel RFPMC wen θ_r is 0, 45, and 90°.

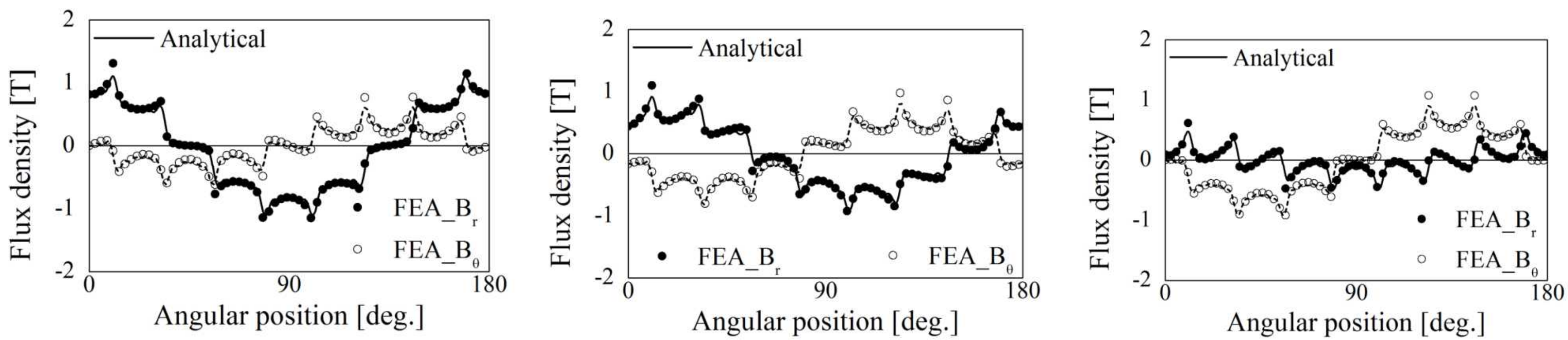

Fig. Comparison of analytical results with FE results for air gap flux density of Halbach RFMC when θ_r is 0°, 45, and 90.

II. Analytical Approach – RFPM Coupling

D. Results

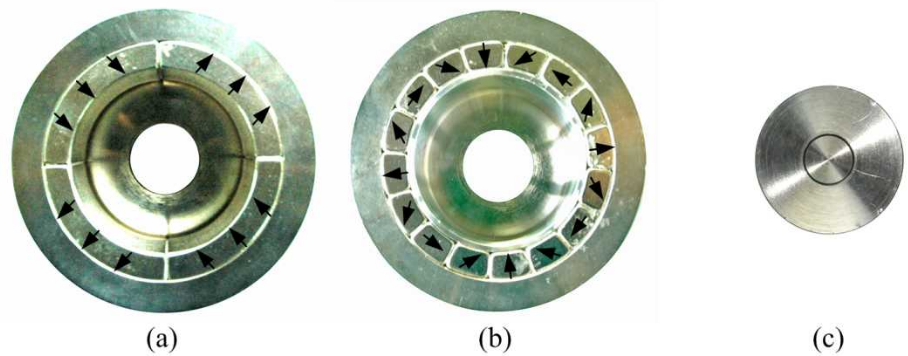

Fig. Actual manufactured RFPMCs; (a) parallel magnetized outer rotor, (b) Halbach magnetized outer rotor and (c) inner rotor.

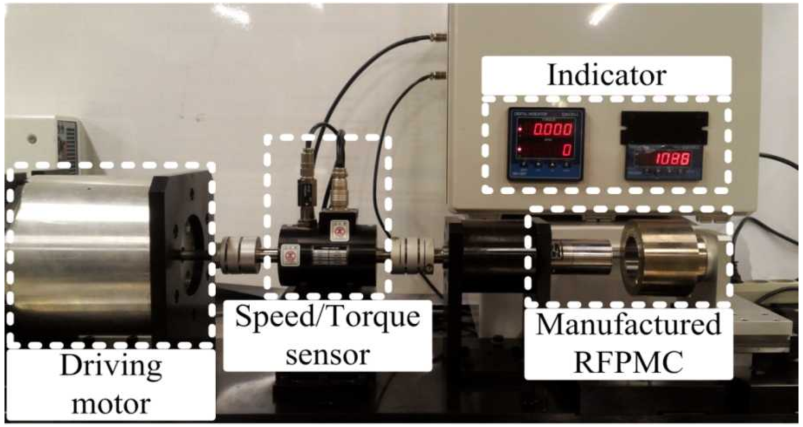

		Analytical results	3D FEA results	Measured results
Parallel magnetization	Torque	16.49 [Nm]	14.71 [Nm]	15.05 [Nm]
	Error	9.6 %	2.3 %	
Halbach magnetization	Torque	19.06 [Nm]	16.72 [Nm]	17.08 [Nm]
	Error	11.6 %	2.1 %	

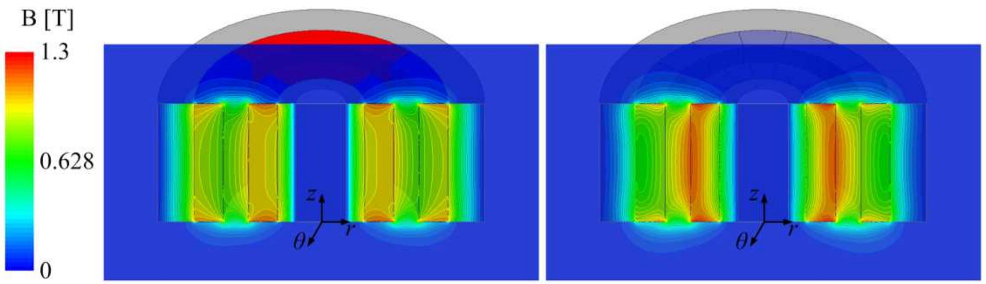

A. Analytical Model

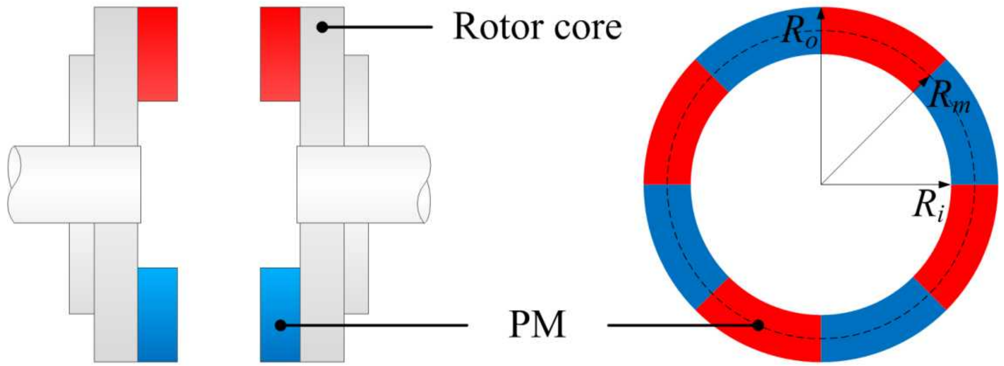

Fig. Schematic diagram of RFPM Coupling

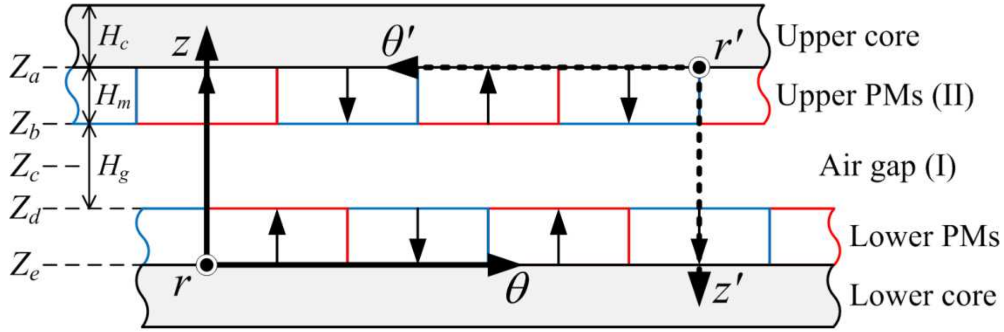

Fig. Analytical Model

B. Magnetization

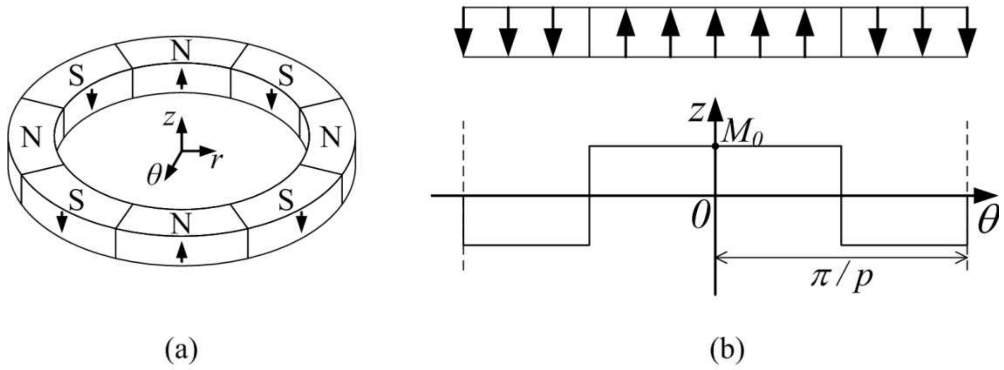

Fig. (a) Axial direction magnetization of AFPMC (b) axial magnetization model for Fourier series expansion.

$$\mathbf{M}_{\mathbf{AF}} = \sum_{n=-\infty,odd}^{\infty} M_{zn} e^{-jnp\theta} \mathbf{i}_{\mathbf{z}}$$

$$M_{zn} = \frac{M_0}{jn\pi}\left(e^{jnp\frac{\theta_w}{2}} - e^{-jnp\frac{\theta_w}{2}} \right)$$

II. Analytical Approach – AFPM Coupling

B. Governing Equations

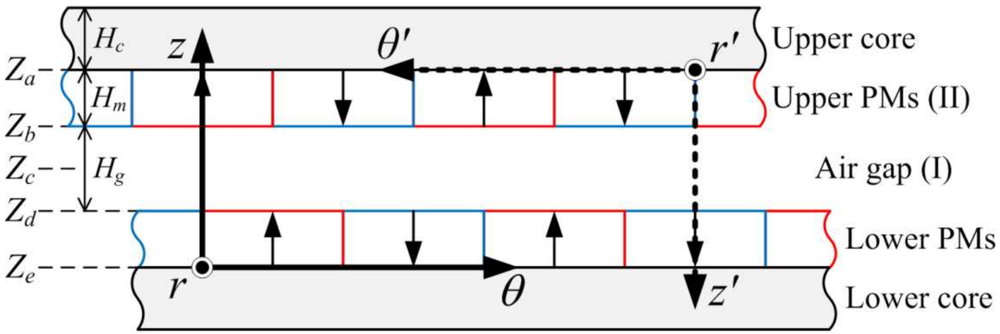

$$\nabla^2 \mathbf{A}^{\mathbf{II}} = -\mu_0 \left(\nabla \times \mathbf{M}_{\mathbf{AF}} \right)$$

$$\nabla^2 \mathbf{A}^{\mathbf{I}} = 0$$

$$\mathbf{A} = \sum_{n=-\infty,odd}^{\infty} A_n(z) e^{-jnp\theta} \mathbf{i_r}$$

$$\mathbf{A}^{\mathbf{I}} = \sum_{n=-\infty,odd}^{\infty} \left(E_n{}^{I} e^{\frac{np}{r}z} + F_n{}^{I} e^{-\frac{np}{r}z} \right) e^{-jnp\theta} \mathbf{i_r}$$

$$\mathbf{A}^{\mathbf{II}} = \sum_{n=-\infty,odd}^{\infty} \left(E_n{}^{II} e^{\frac{np}{r}z} + F_n{}^{II} e^{-\frac{np}{r}z} - \frac{j\mu_0 r}{np} M_{zn} \right) e^{-jnp\theta} \mathbf{i_r}$$

$$\mathbf{B_z} = \sum_{n=-\infty,odd}^{\infty} \frac{jnp}{r} A_n(z) e^{-jnp\theta} \mathbf{i_z}$$

$$\mathbf{B_\theta} = \sum_{n=-\infty,odd}^{\infty} \frac{\partial}{\partial z} A_n(z) e^{-jnp\theta} \mathbf{i_\theta}$$

$$\mathbf{B_{tz}}^{\mathbf{Z_a}} = \left\{ \mathbf{B_z}^{\mathbf{II}} \left(r, \theta, Z_a \right) + \mathbf{B_z}^{\mathbf{I}} \left(r', \theta', 0 \right) \right\}$$

$$\mathbf{B_{t\theta}}^{\mathbf{Z_a}} = \left\{ \mathbf{B_\theta}^{\mathbf{II}} \left(r, \theta, Z_a \right) + \mathbf{B_\theta}^{\mathbf{I}} \left(r', \theta', 0 \right) \right\}$$

C. Boundary Conditions

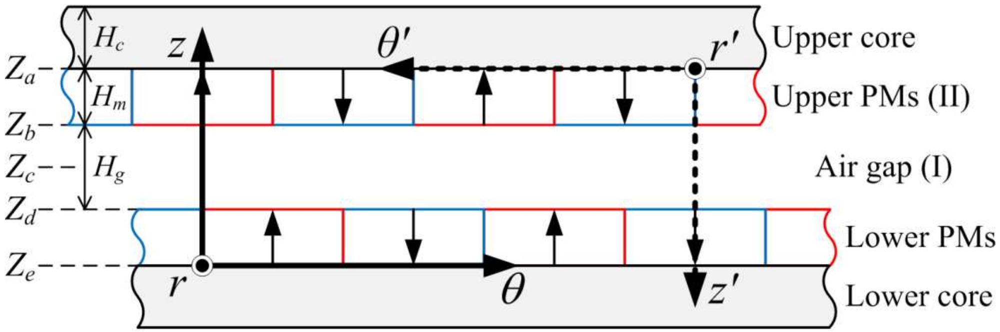

$$\mathbf{B}_\theta^{\mathrm{II}}(r,\theta,Z_a)=0$$

$$\mathbf{B}_\theta^{\mathrm{I}}(r,\theta,Z_e)=0$$

$$\mathbf{B}_z^{\mathrm{I}}(r,\theta,Z_b)=\mathbf{B}_z^{\mathrm{II}}(r,\theta,Z_b)$$

$$\mathbf{B}_\theta^{\mathrm{I}}(r,\theta,Z_b)=\mathbf{B}_\theta^{\mathrm{II}}(r,\theta,Z_b)$$

II. Analytical Approach – AFPM Coupling

D. Results

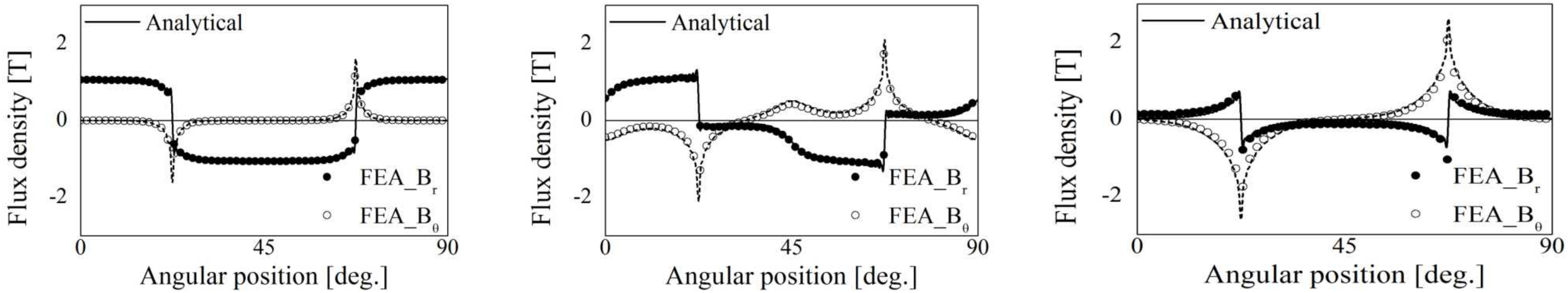

Fig. Comparison of analytical results with 3D FE results for air gap flux density at $g = 4$ mm when θ_a is 0, 22.5°, 45.

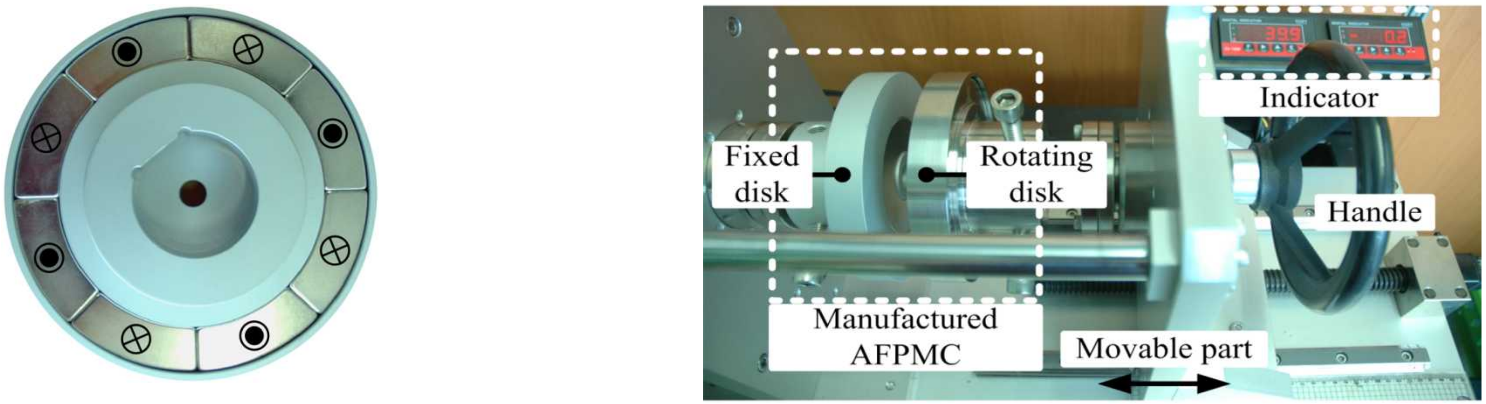

Fig. Testing apparatus for torque measurement of AFPMC.

II. Analytical Approach – AFPM Coupling

D. Results

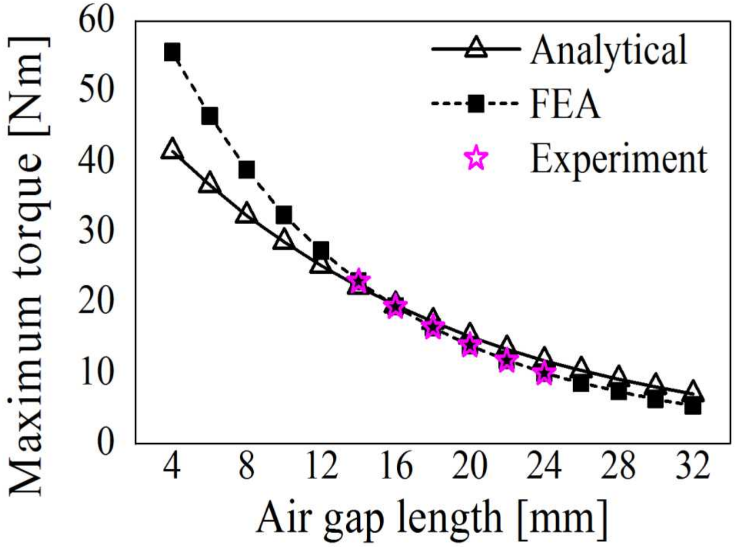

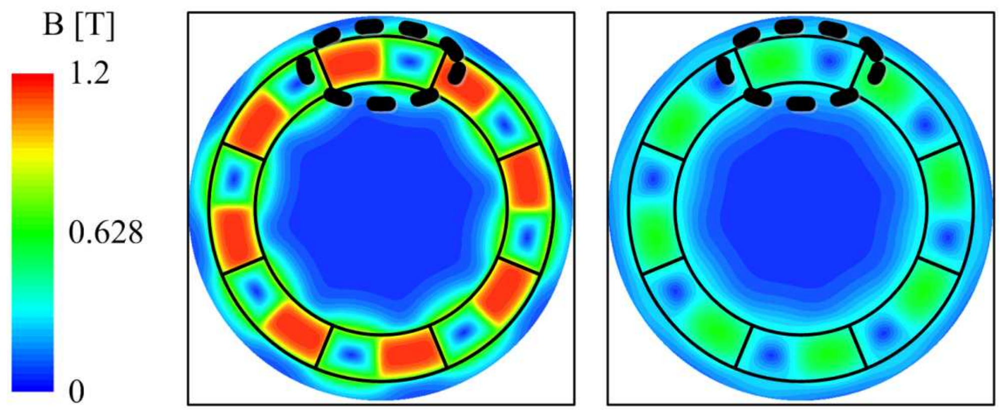

Fig. Magneto-static field distributions obtained from 3D FE analysis at θ_a = 22.5°; (a) g = 4 mm and (b) g = 16 mm.

III Analytical Approach - Gears

III. Analytical Approach – Gears

A. Analytical Model

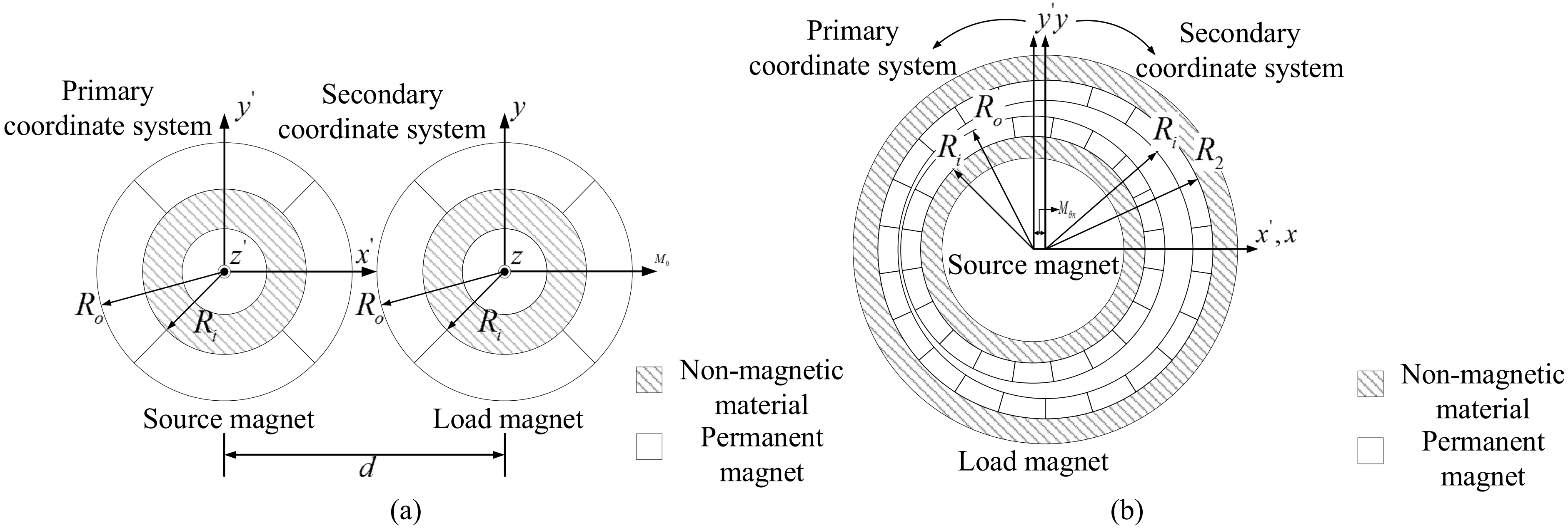

Fig. 6 Schematic diagram of (a) magnetic spur gear (b) magnetic cycloid gear

III. Analytical Approach – Gears

- The analysis of magnetic gear is implemented in three parts :

① Analysis of magnetic fields produced by source magnet
② Coordinate conversion
③ Torque calculation by using Lorentz force

B. Analytical model

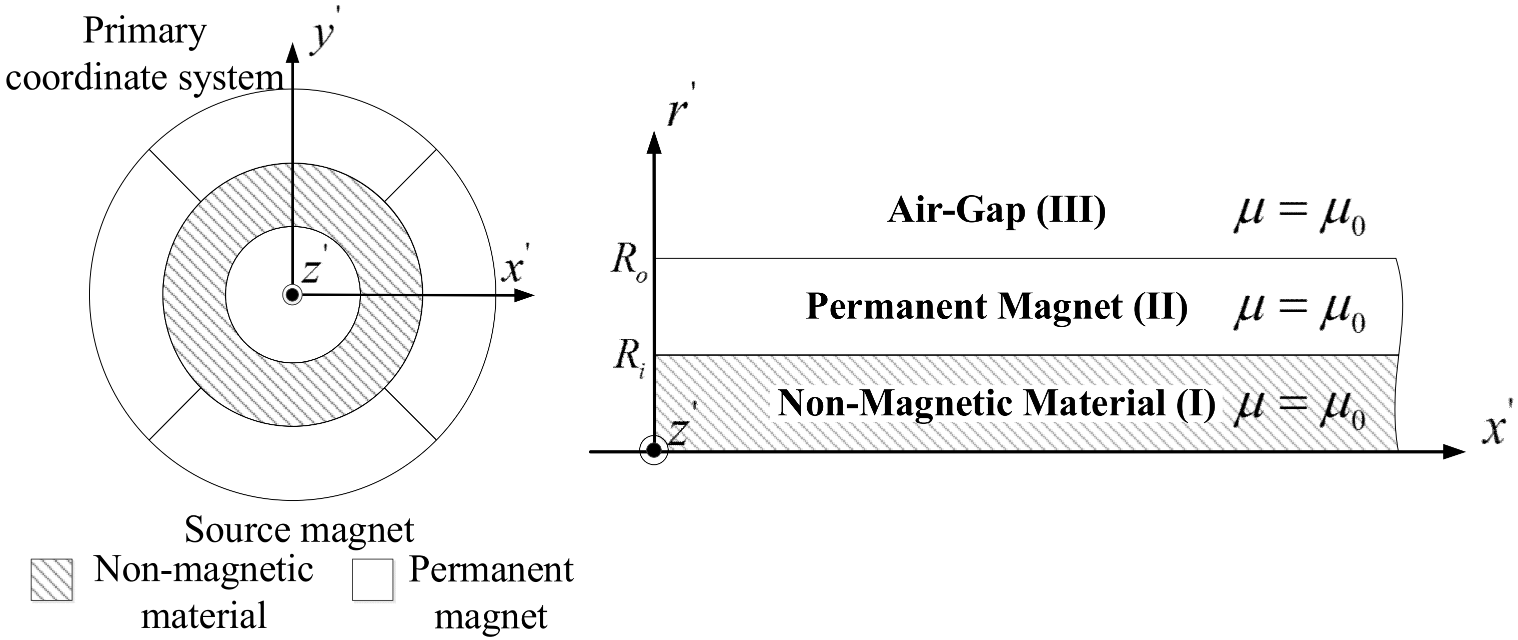

Fig. Magnetic field analysis model of the source magnet

C. Magnetization model

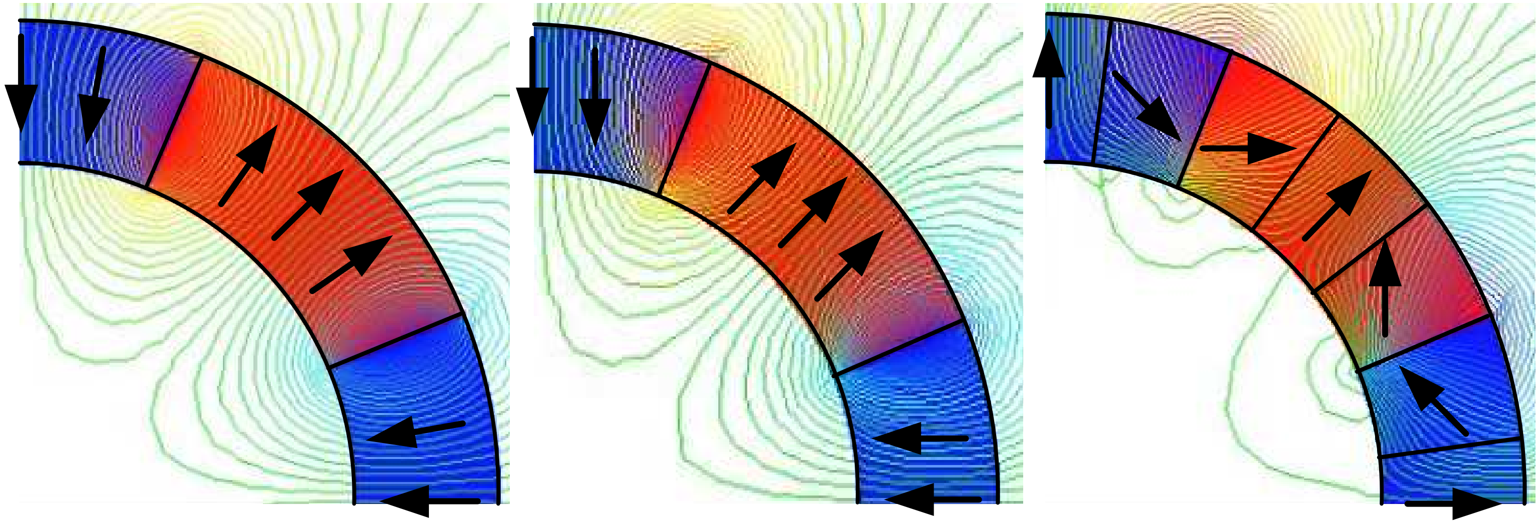

(a) (b) (c)

Fig. Magnetization of magnets : (a) radial magnetization (b) parallel magnetization (c) 3-segments Halbach magnetization

III. Analytical Approach – Gears

D. Magnetic field calculations – governing equations

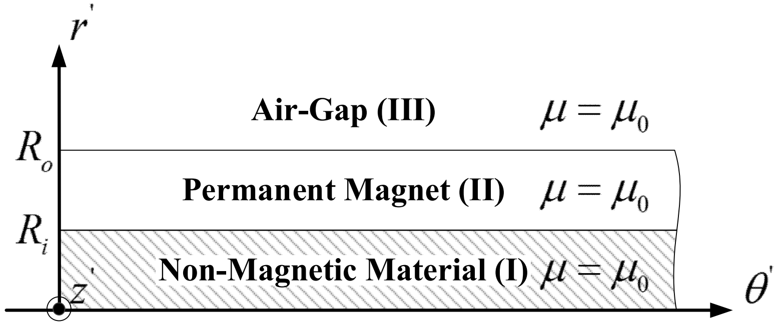

Fig. 12 Analytical model

$$\mathbf{A} = \sum_{n=-\infty,odd}^{\infty} A_n(r)e^{-jnp_s(\theta')} \cdot \mathbf{i_z}$$

$$\mathbf{A}^{I,III} = \sum_{n=-\infty,odd}^{\infty} \left\{ C_n^{\ I,III} r^{np_s} + D_n^{\ I,III} r^{-np_s} \right\} \cdot e^{-jnp_s\theta'} \mathbf{i_z}$$

$$\mathbf{A}^{II} = \sum_{n=-\infty,odd}^{\infty} \left\{ \begin{array}{l} C_n^{\ II} r^{np_s} + D_n^{\ II} r^{-np_s} \\ -\dfrac{\mu_0 (jnp_s M_{rn} + M_{\theta n})}{1-(np_s)^2} r \end{array} \right\} \cdot e^{-jnp_s\theta'} \mathbf{i_z}$$

$$\mathbf{B} = \mu_0 (\mathbf{H} + \mathbf{M})$$

$$\nabla \times \mathbf{B} = \nabla \times \mu_0 \mathbf{M},$$

$$\mathbf{B} \equiv \nabla \times \mathbf{A}$$
$$\nabla \cdot \mathbf{A} = 0$$

$$\nabla^2 \mathbf{A}^{I,III} = 0$$

$$\nabla^2 \mathbf{A}^{II} = -\mu_0 (\nabla \times \mathbf{M})$$

$$\mathbf{B} \equiv \nabla \times \mathbf{A}$$

$$\mathbf{B_{r'}}^{\mathbf{III}} = -\sum_{n=-\infty}^{\infty} \frac{jnp_s}{r'} A_n^{\ III}(r') e^{-jnp_s\theta'} \mathbf{i_r}$$

$$\mathbf{B_{\theta'}}^{\mathbf{III}} = -\frac{\partial}{\partial r} \sum_{n=-\infty}^{\infty} \frac{jnp_s}{r'} A_n^{\ III}(r') e^{-jnp_s\theta'} \mathbf{i}_\theta$$

D. Magnetic field calculations – boundary conditions

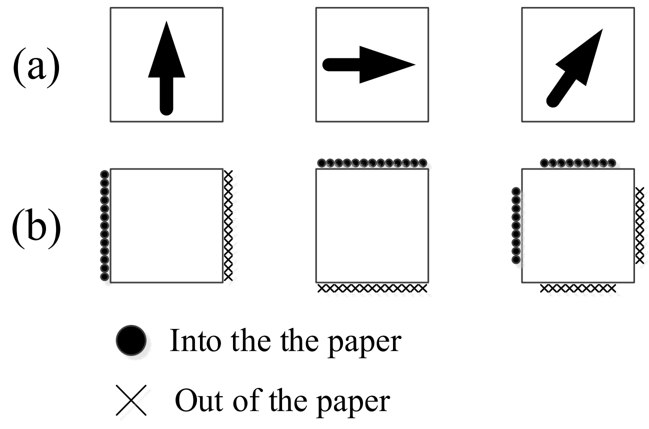

Fig. Electromagnetic dual of any magnetization : (a) direction of magnetization (b) equivalent current model

1) $\lim_{r \to 0} A_n^{I}(r,\theta) = 0$ and $\lim_{r \to \infty} A_n^{III}(r,\theta) = 0$

2) $B_{r'n}^{I}(R_i,\theta') = B_{r'n}^{II}(R_i,\theta')$ at $r = R_i$

$B_{\theta' n}^{I}(R_i,\theta') - B_{r'n}^{II}(R_i,\theta') = -\mu_o M_{\theta n}$

3) $B_{r'n}^{II}(R_o,\theta') = B_{r'n}^{III}(R_o,\theta')$ at $r = R_o$

$B_{\theta' n}^{II}(R_o,\theta') - B_{r'n}^{III}(R_o,\theta') = \mu_o M_{\theta n}$

J. Y. Choi, H. Y. Kim, S. M. Jang, S. H. Lee, "Thrust Calculations and Measurements of Cylindrical Linear Actuator Using Transfer Relations Theorem," *IEEE Trans. Magn.*, vol.44, pp.4081-4084, Nov. 2008.

E. Coordinate conversion

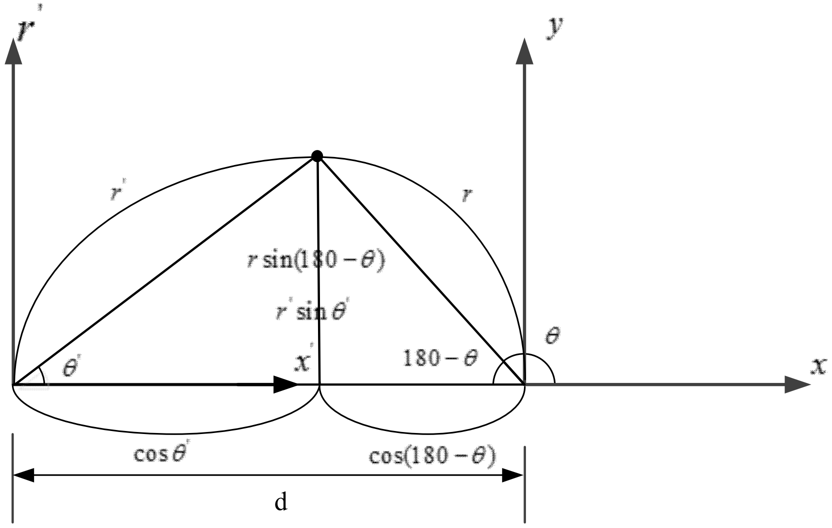

Fig. Schematic of coordinate conversion

$$r' \sin\theta' = r\sin(180-\theta)$$
$$d = r' \cos\theta' + r\cos(180-\theta)$$

$$r' = \sqrt{r^2 + 2rd\cos(\theta) + d^2}$$
$$\theta' = \arctan\left(\frac{r\sin(\theta)}{r\cos(\theta)+d}\right)$$

III. Analytical Approach – Gears

E. Coordinate conversion

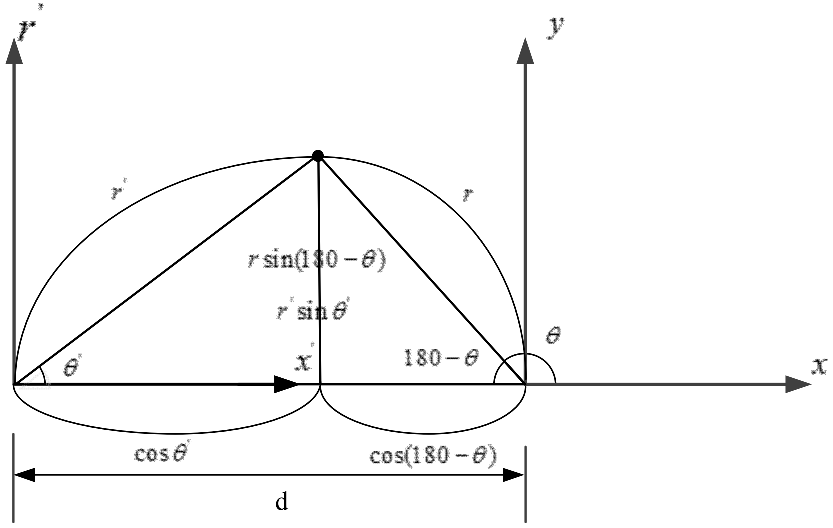

Fig. Schematic of coordinate conversion

$$B_{r'}^{III}(r',\theta') \qquad B_{\theta'}^{III}(r',\theta') \quad \Rightarrow \quad B_{r'}^{III}(r,\theta) \qquad B_{\theta'}^{III}(r,\theta)$$

$$B_x^{ext} = \begin{matrix} B_{r'}^{III}(r,\theta)\cdot\cos\left\{\arctan\left(\dfrac{r\sin\theta}{r\cos\theta+d}\right)\right\} \\ -B_{\theta'}^{III}(r,\theta)\sin\left\{\arctan\left(\dfrac{r\sin\theta}{r\cos\theta+d}\right)\right\} \end{matrix}$$

$$B_y^{ext} = \begin{matrix} B_{r'}^{III}(r,\theta)\cdot\sin\left\{\arctan\left(\dfrac{r\sin\theta}{r\cos\theta+d}\right)\right\} \\ +B_{\theta'}^{III}(r,\theta)\cos\left\{\arctan\left(\dfrac{r\sin\theta}{r\cos\theta+d}\right)\right\} \end{matrix}$$

The Cartesian coordinate is common to both systems

F. Torque Analysis

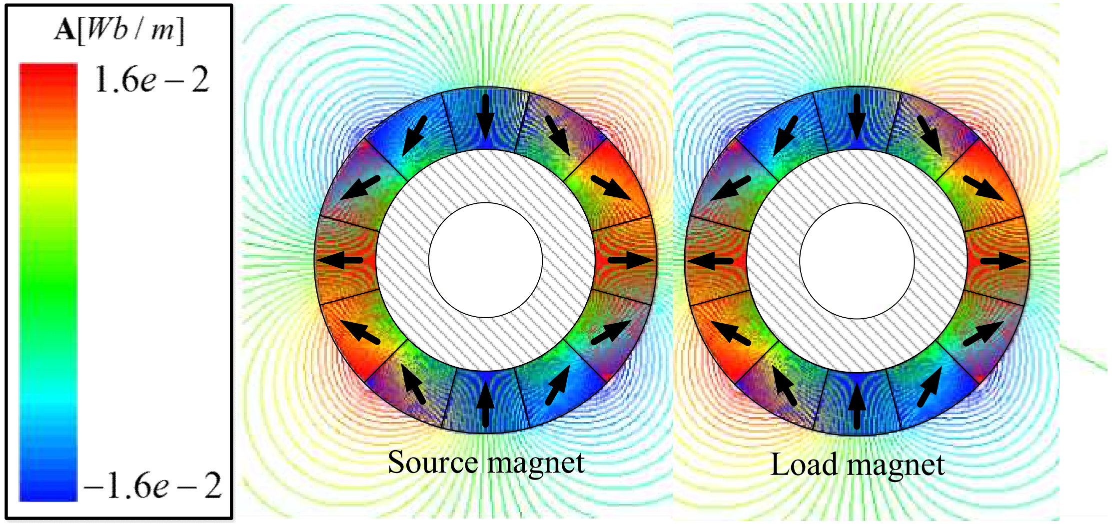

Fig. Torque computed on currents in the external field

$$d\mathbf{T} = \mathbf{r} \times (\mathbf{J} \times \mathbf{B}_{ext})dV$$

$$\mathbf{T} = \int_S \mathbf{r} \times (\mathbf{j}_m \times \mathbf{B}_{ext})da$$

$$\mathbf{j}_m = \mathbf{M} \times \mathbf{n}$$

$$\boxed{\mathbf{J}_m = \nabla \times \mathbf{M} = 0}$$

F. Torque Analysis

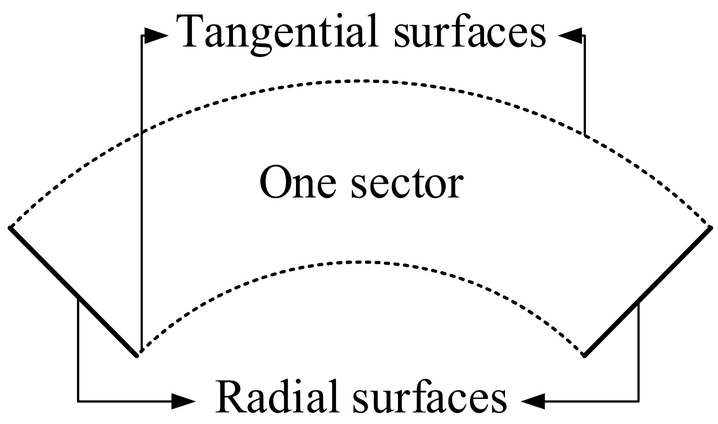

Fig. The radial surface torque and the tangential surface torque

$$T(\theta) = T_r(\theta) + T_{t1}(\theta) + T_{t2}(\theta)$$

$$T_r(\theta) = \begin{array}{l} 2M\cos\left(\dfrac{\pi}{2p_l}\right) L \dfrac{(R_2 - R_1)}{N_r} \displaystyle\sum_{p=0}^{2p_l-1} \sum_{q=0}^{Nr} (-1)^p S_r(q) r(q) \\ \times[\cos(\theta_{edge}(\theta,p)) B_x^{ext}(r, \theta_{edge}(\theta,p)) \\ + \sin(\theta_{edge}(\theta,p)) B_y^{ext}(r, \theta_{edge}(\theta,p))] \end{array}$$

$$T_{t1}(\theta) = \begin{array}{l} -ML \dfrac{R_1(\frac{\pi}{p_l})}{N_t} \displaystyle\sum_{p=0}^{2p_l-1} \sum_{q=0}^{N_t} (-1)^p S_r(q) R_1 \sin(\theta(q)) \\ \times[\cos(\theta(q) + p\dfrac{\pi}{p_l} + \theta) B_x^{ext}(R_1, \theta(q) + p\dfrac{\pi}{p_l} + \theta) \\ + \sin(\theta(q) + p\dfrac{\pi}{p_l} + \theta) B_y^{ext}(R_1, \theta(q) + p\dfrac{\pi}{p_l} + \theta)] \end{array}$$

$$T_{t2}(\theta) = \begin{array}{l} ML \dfrac{R_2(\frac{\pi}{p_l})}{N_t} \displaystyle\sum_{p=0}^{2p_l-1} \sum_{q=0}^{N_t} (-1)^p S_r(q) R_2 \sin(\theta(q)) \\ \times[\cos(\theta(q) + p\dfrac{\pi}{p_l} + \theta) B_x^{ext}(R_2, \theta(q) + p\dfrac{\pi}{p_l} + \theta) \\ + \sin(\theta(q) + p\dfrac{\pi}{p_l} + \theta) B_y^{ext}(R_2, \theta(q) + p\dfrac{\pi}{p_l} + \theta)] \end{array}$$

III. Analytical Approach – Gears

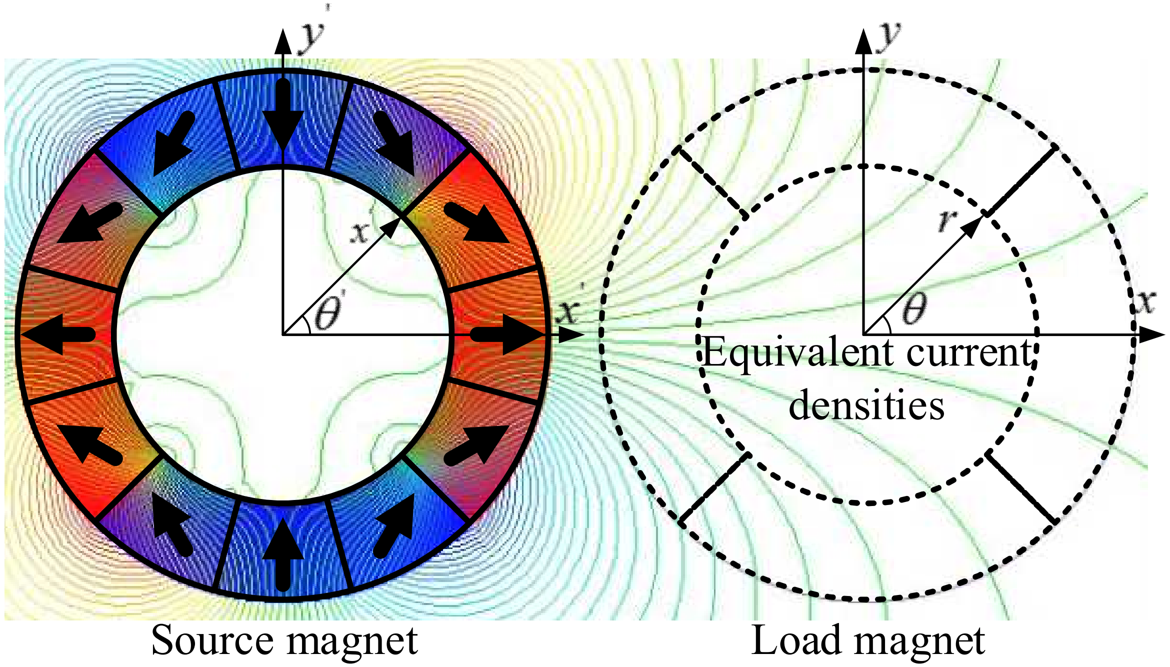

Fig. 21 Magnetic flux line distribution of 3-segments Halbach magnetic spur gear

III. Analytical Approach – Gears

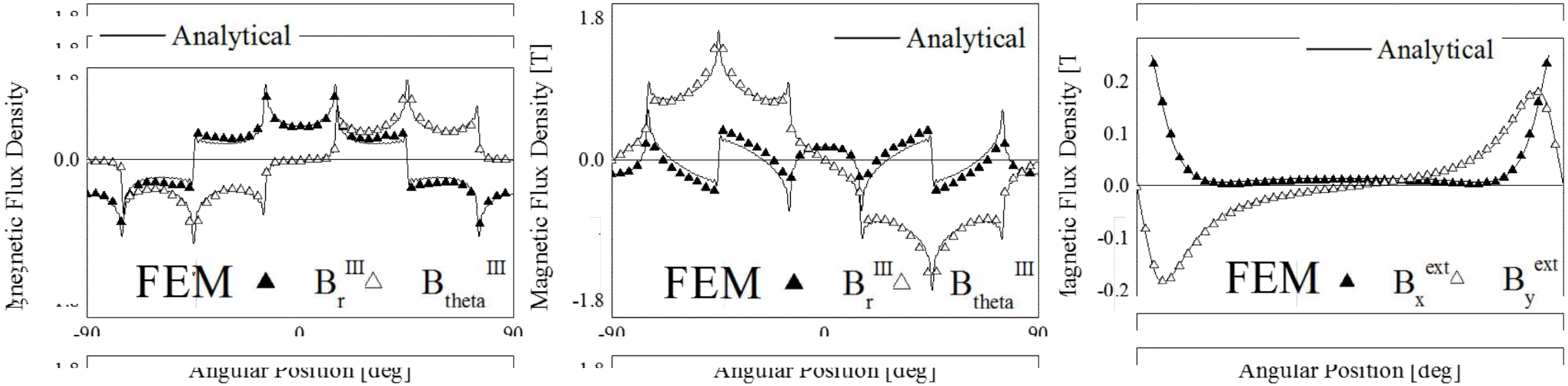

(a) (b) (c)

Fig. Comparison of magnetic flux density between the analytical calculations and 2D FE analysis for Halbach spur gear (a) at $r' = 35mm$ (b) at $r' = 55mm$ (c) at $r = 60mm$

III. Analytical Approach – Gears

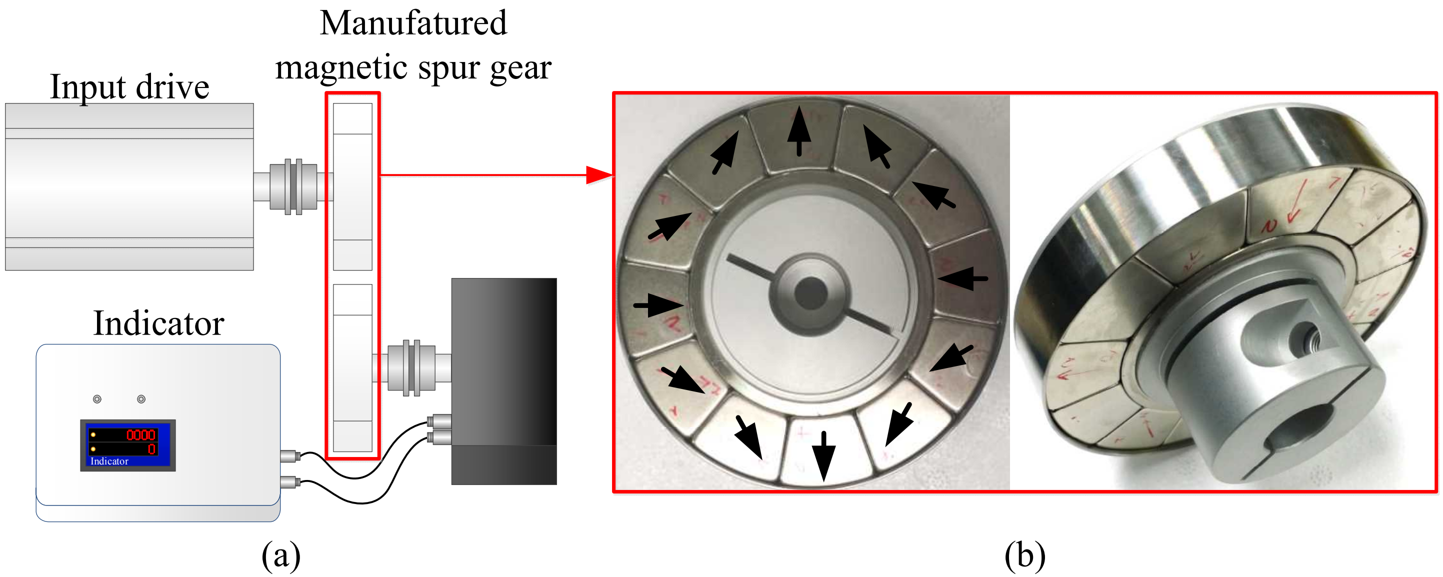

Fig. (a) Test apparatus for torque measurement (b) Manufactured magnetic spur gear with Halbach magnetized PMs.

III. Analytical Approach – Gears

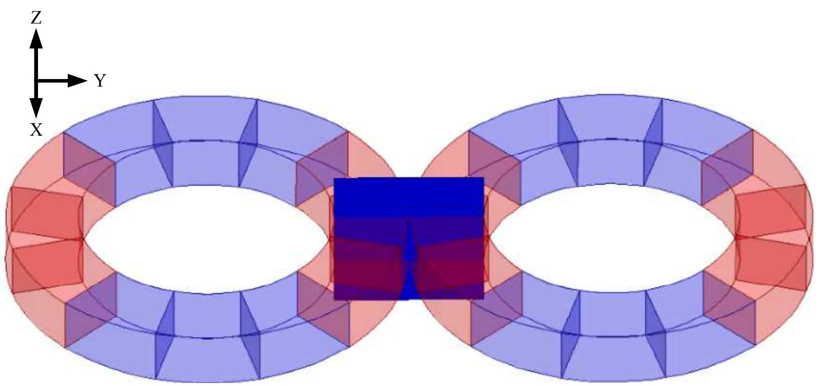

Fig. 3D FE analysis model of magnetic spur gear

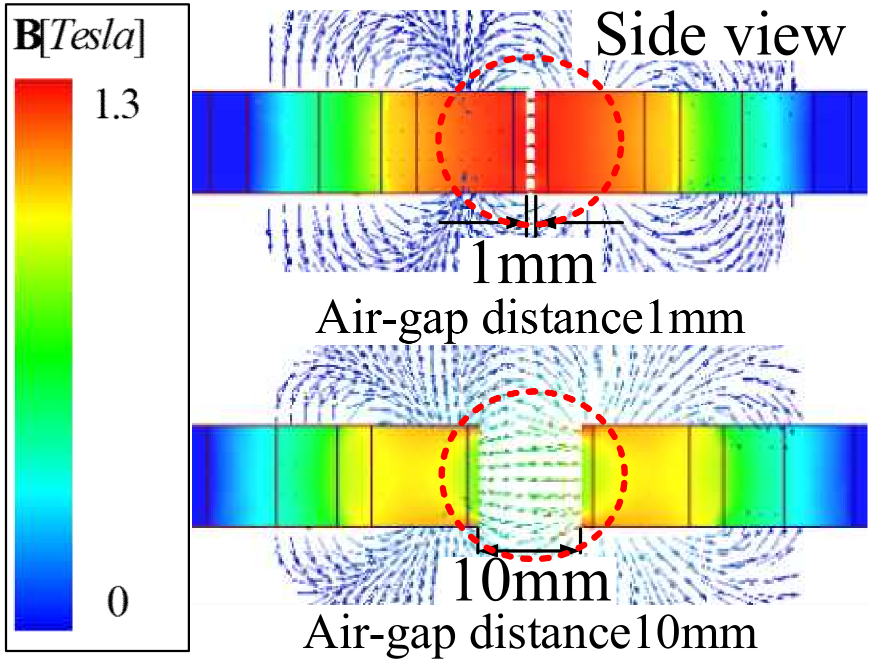

Fig. 3D effect on magnetic spur gear with 3-segments Halbach magnetized PMs

Magnetization	Air-gap distance	Analytical result (error)	2D FE result (error)	Measurement
Halbach	1mm	13 [Nm] (26%)	13.4 [Nm] (30%)	10.29 [Nm]
Halbach	10mm	9.4 [Nm] (52%)	9.9 [Nm] (60%)	6.17 [Nm]

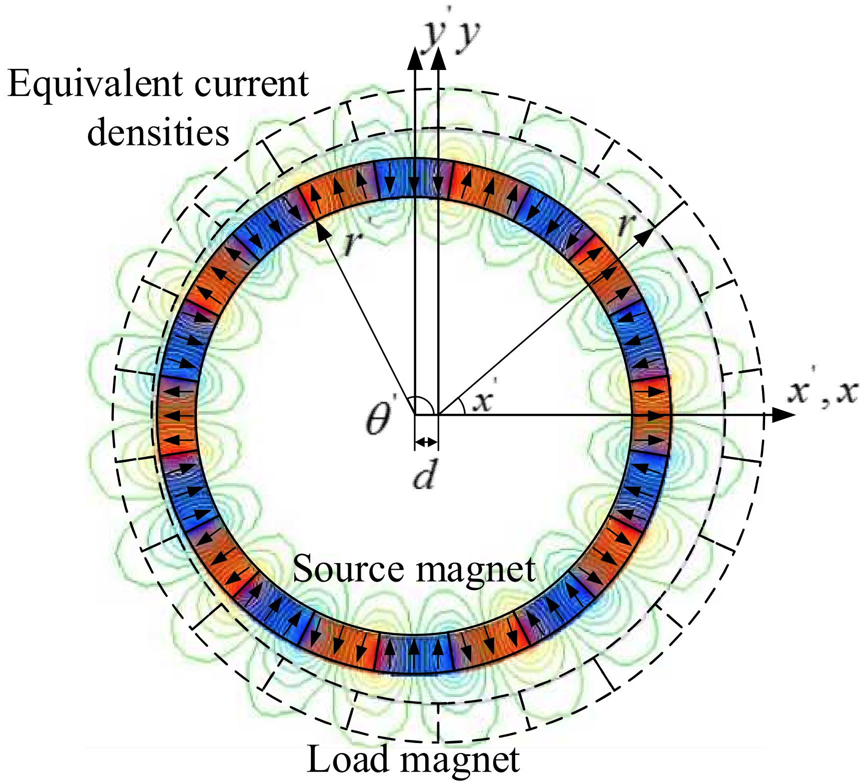

Fig. 28 Magnetic flux line distribution of parallel magnetic cycloid gear $d = 2.5mm$

III. Analytical Approach – Gears

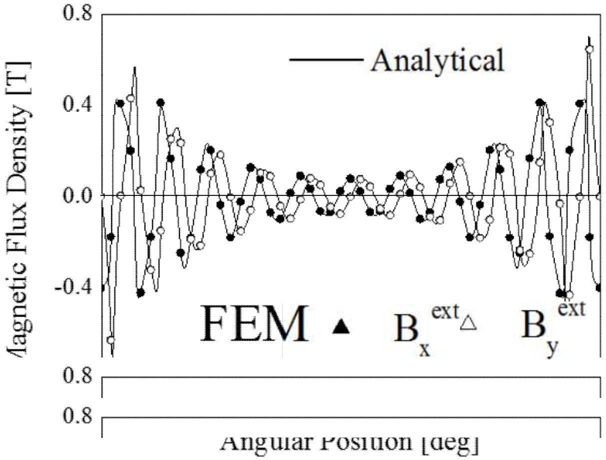

(a)

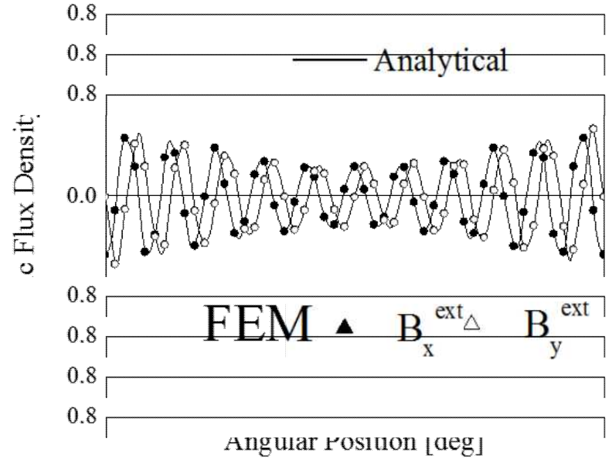

(b)

Fig. Comparison of magnetic flux density of magnetic cycloid gear with parallel magnetized PMs between the analytical calculations and 2D FEA when $r = 30mm$, (a) $d = 2.5mm$ (b) $d = 1mm$

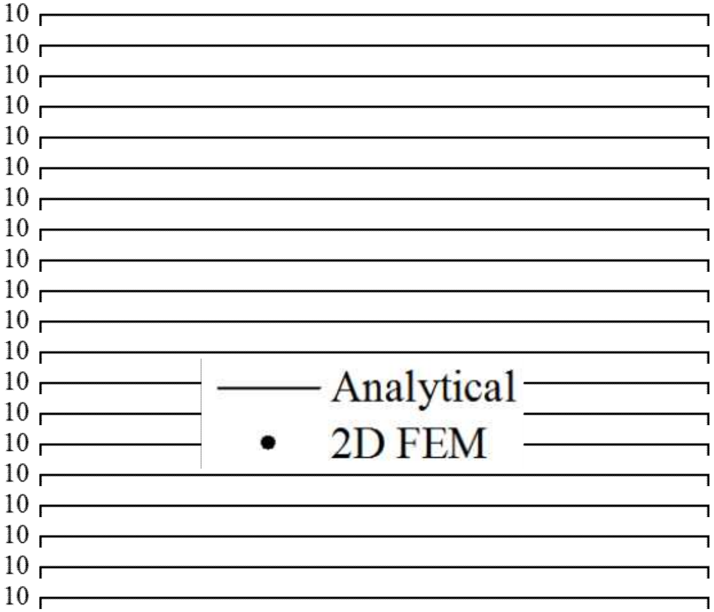

Fig. Comparison of the torque calculation and FE results, when $d = 2.5mm$

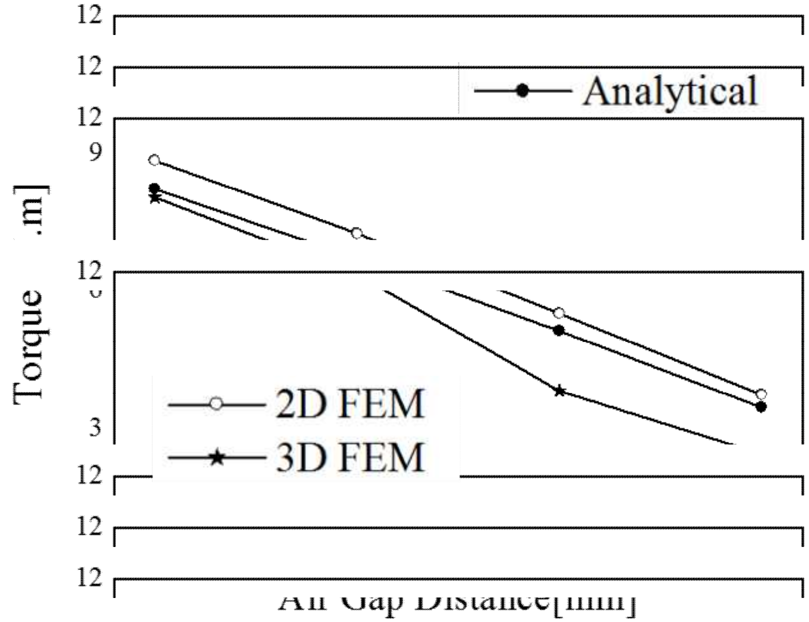

Fig. Comparison of the torque calculation and FE results, when $1\text{mm} \le d \le 2.5mm$

IV Conclusion

IV. Conclusion

- The analytical torque calculation for a magnetic and coupling is presented and compared with the 2D, 3D FE and experimental results
- The analytical results are shown in good agreement with the 2D FEA results.
- However, the analytical results are different from experimental results and 3D FE results
- Difference of torque results are caused by 3D effects
- The percentage of error between the analytical results and measurement, 3D FE results should increase when the air-gap distance is enlarged.
- In spite of the 3D effects, It would be possible to use these analytical calculations for initial design and optimization purposes.

Thank you for your attention